



New Layer Coefficients for Geogrid-Reinforced Pavement Bases

Sireesh Saride¹ · Ramu Baadiga¹

Received: 30 August 2020 / Accepted: 11 December 2020 / Published online: 8 February 2021
© Indian Geotechnical Society 2021

Abstract Stabilizing the base layers of flexible pavements is gaining tremendous attention due to the lack of suitable construction materials. A geogrid reinforcement could offer a reduction in granular layer thickness or enhance the service life of the pavement. However, there is no standard direct methodology available for the design of a flexible pavement with a geogrid-reinforced base layer. The current design approaches adopt the base layer coefficient ratio (*LCR*) derived from the layer coefficient equation proposed by the American Association of State Highway and Transportation Officials (AASHTO 1993), which was initially developed for an unreinforced base layer. Moreover, the accuracy of the existing model for determining the base layer coefficient needs a reassessment since it varies for different subgrade conditions. Hence, an attempt was made to propose a new model which emphasizes on unreinforced and geogrid-reinforced base layer coefficients for weak-to-moderate subgrade conditions. Prior to the analysis, large-scale model pavement experiments were conducted to realize modulus improvement factor (*MIF*) and range of values of *LCR* of different geogrids, which are crucial parameters used in the design. In addition, design examples, validation and the *MIF* and *LCR* values of geogrid-reinforced base layer were provided for obtaining the base layer coefficients. It was noticed that the *MIF* and *LCR* value for the geogrid-reinforced base layers range between 1.6–3.33 and 1.23–1.59, respectively. The newly proposed equation for the base layer coefficients accounted for about a 33% reduction in the base layer thickness compared to

the unreinforced case. Hence, a safe and economical pavement section may be obtained from the proposed model.

Keywords Subgrade · Geogrid · Modulus improvement factor · Layer coefficient ratio · Base layer coefficients · Pavement design

List of Symbols

a	Radius of circular loading plate
a_1, a_2	Layer coefficients of asphalt and base layers
a_{2r}	Base layer coefficient of reinforced section
a_{2u}	Base layer coefficient of unreinforced section
d_1, d_2	Asphalt and base layer thicknesses
d_{2r}	Reinforced base layer thickness
D	Diameter of circular plate
E_1	Elastic modulus of layer 1 (base and subbase together)
E_2	Elastic modulus of layer 2 (subgrade)
$E_{bcr} = E_{1r}$	Elastic modulus of reinforced base course
$E_{bcu} = E_{1u}$	Elastic modulus of unreinforced base course
E_{eq}	Equivalent elastic modulus
S_e	Elastic settlement of plate
ε_t	Horizontal tensile strain below the asphalt layer (fatigue strain)
ε_v	Vertical compressive strain on top of the subgrade (rutting strain)
I	Influence factor
I_f	Improvement factor
μ	Poisson's ratio
H	Total height of base and subbase layers
H_1	Base layer thickness
H_2	Subbase layer thickness
H_3	Subgrade layer thickness

✉ Sireesh Saride
sireesh@ce.iith.ac.in

¹ Department of Civil Engineering, Indian Institute of Technology Hyderabad, Sangareddy 502 285, India

m_2	Drainage coefficient of base layer
M_{ra}	Resilient modulus of asphalt layer
M_{rr}	Improved resilient modulus
M_{rs}	Subgrade resilient modulus
M_{ru}	Resilient modulus of unreinforced base layer
q	Bearing pressure
S_N	Required structural number
S_{Na}	Actual structural number
S_o	Overall standard deviation
Z_R	Standard normal deviate
ΔPSI	Allowable loss of serviceability

Introduction

After the concrete industry, road construction consumes a large quantity of aggregate material from the quarries. The global agencies and local practitioners are alarmed about the shortage of crushed aggregate materials. Besides, stabilizing the base layers of flexible pavements with geogrids is gaining tremendous attention due to the lack of suitable construction materials. The usage of geogrids in the base layer is highly recommended, primarily due to the reinforcement function, in recent years, over conventional methods such as chemical stabilization. Geogrids are considered to play a vital role in three ways, i.e., arresting the lateral movement of aggregate material, sustaining higher loads and giving adequate membrane support over induced loads. These leading advantages due to geogrids are considered to aid in the reduction in base course thickness substantially [1–3]. However, the benefit that comes from the geogrid material was limited to certain conditions, especially the type of subgrade and the resistance offered by it. For example, Hufenus et al. [4] observed that the reinforcement is beneficial with subgrade possessing California bearing ratio (CBR) of less than or equal to 6% beyond which a marginal improvement was reported. A similar study by Christopher [5] observed minimal reinforcement effect beyond subgrade CBR of 8%. Generally, the benefit availed due to geogrid is classified in terms of bearing pressure improvement factor, layer coefficient ratio (*LCR*) and traffic benefit ratio (*TBR*), mainly with significant emphasis on *LCR*, though it is not a direct approach to determine the influence of reinforcement. The layer coefficient ratio is defined as the ratio of the reinforced base layer coefficient to the base layer coefficient of an unreinforced base with the same material properties and thicknesses, and this will be further discussed in detail in the subsequent sections. The traffic benefit ratio is defined as a ratio of a number of load cycles applied on a reinforced pavement section to an

unreinforced pavement section, for a given settlement amount. However, these approaches are being less implemented due to a lack of experimental data and design methods [6]. Only few studies [7, 8] reported *LCR* values based on the analytical solution or backward analysis from field measured data. Recently, Goud et al. [9] have demonstrated the procedure to establish the *LCR* values based on controlled large-scale experimental studies. They provided a range of *LCR* values (1.1–1.3) to be adopted in the design of flexible pavements with geogrid-reinforced base layers. The range of *LCR* values for geogrids having the tensile strength in the range of 15–30 kN/m varied between 1.1 and 2.0 [3, 9].

Typically for a flexible pavement, two factors are used to incorporate the benefits of geosynthetics in the pavement design, i.e., *LCR* and *TBR* [6]. These benefit factors aid in lending reduced base layer thickness and increased service life of the pavement. The concept of *LCR* was introduced to enable the use of geosynthetic reinforcement [10]. However, there is no standard direct methodology available for the design of a flexible pavement with a geogrid-reinforced base layer, as there is no methodology available to assess the base layer coefficients directly. The existing guidelines provided by the American Association of State Highway and Transportation Officials (AASHTO) [11] and Indian Roads Congress (IRC) [12] have suggested adopting an *LCR*-based design, which will accommodate the benefits of geosynthetics in terms of modulus improvement factor (*MIF*). On the other hand, mechanistic-empirical (M-E) pavement design guidelines do not count for the inclusion of geosynthetics in base layers [13]. Thus, still, modified AASHTO guidelines give consistent results and follow the M-E principles but not to the full extent [13].

The current design methods [12, 14] adopt an equation to determine the base layer coefficients proposed by AASHTO [11], which was developed for an unreinforced granular base layer [15]. Since there is no direct procedure available for obtaining *LCR* values of a particular geosynthetics material, back-calculation procedures were followed based on *MIF*. The equation suggested by Giroud and Han [15] for determining *LCR* based on *MIF* value considers the existing AASHTO base layer equation (Eq. 1), which was initially proposed based on the American Association of State Highway Officials (AASHO) road tests in late 1950s.

$$a_2 = 0.249 \times \log_{10}(M_{rbc}) - 0.977, \quad (\text{AASHTO}[11]) \quad (1)$$

where a_2 is the base layer coefficient, M_{rbc} is the resilient modulus of unreinforced base layer, in psi.

The accuracy of the existing equation needs a reassessment since the current equation has been adopted for wide range of subgrade conditions, with different CBR values. An appropriate equation for a range of subgrade

conditions, especially for geogrid-reinforced base layer sections, might lead to a safe and economical pavement design. Moreover, the AASHTO guidelines consider the structural number-based design; it is not always assessed whether the designed section is safe against horizontal tensile strain below the asphalt layer (fatigue) and vertical compressive strains on the top of the subgrade (rutting) [16–18].

Hence, an attempt was made to verify the existing base layer equation of the unreinforced section first and subsequently propose a new equation by considering a weak to moderate subgrade conditions (CBR of 2–5%). Once the newly proposed base layer coefficient equation was validated for unreinforced bases, an attempt was made to propose a new equation to obtain the base layer coefficients for the geogrid-reinforced section based on *LCR* value. Along with the developed equations, a chart was provided to directly obtain the reinforced base layer coefficient by considering the *LCR* values, unreinforced resilient modulus. A typical design chart was also provided to deduce the granular layer thickness (base and subbase layers together) for a given set of *LCR*, M_{ru} and design traffic conditions. Prior to the analysis, large-scale model pavement experiments (LSMPE) were conducted to ascertain the *MIF* and *LCR* values, which are crucial parameters used in the design and to understand the practical range of these design parameters.

Materials and Methods

Subgrade Material

Based on a preliminary examination, the required quantity of subgrade material was sourced from the vicinity of IIT Hyderabad campus. Prior to the engineering testing, subgrade material was thoroughly pounded and dried. The essential physical and mechanical soil properties were determined in the laboratory. The physical and mechanical properties of subgrade material are listed in Table 1. As

Table 1 The laboratory determined properties of subgrade material

Properties	Value	Standard
Specific gravity (G_s)	2.71	IS:2720 [19]
Liquid limit (LL), %	48	IS:2720-5 [20]
Plastic limit (PL), %	24	
Plasticity index (PI), %	24	
Differential free swell index, %	15	IS:2720-40 [21]
Maximum dry unit weight (MDU), kN/m^3	19	IS:2720-7 [22]
Optimum moisture content (OMC), %	14.5	
Soil classification	SC	IS:1498 [23]

listed in Table 1, the subgrade soil has a slightly higher liquid limit (LL = 48%) value; hence, free-swell index test was conducted as per IS: 2720-40 [21]. The differential free-swell index was found to be minimal at 15% against moisture contact. Further, the grain size distribution assessed by wet sieving revealed that the percentage finer passing 75 microns IS sieve was 50%. Hence, in addition to the wet sieving, hydrometer analysis was also performed to obtain the complete grain size distribution. From the hydrometer analysis, the percentage of silt and clay presented in the entire sample was of the order of 23% and 27%, respectively. Based on the index properties and grain size analyses, the soil is classified as “clayey sand” as per the IS:1498-1970 [22]. According to the Unified Soil Classification System, the subgrade soil can be classified as ‘lean clay.’ The grain size distribution plot of the soil sample is shown in Fig. 1.

The subgrade soil was further examined for optimum moisture content and dry unit weight relation in compliance with IS:2720-7 [23]. Since the significant portion of the subgrade material consisted of fines content, the lightweight Proctor compaction test was performed. The characteristic compaction curve of subgrade material is shown in Fig. 2. The subgrade soil has a maximum dry unit weight (MDU) of 19 kN/m^3 and an optimum moisture content (OMC) of 14.5%.

Determination of Targeted Subgrade CBR Values

As the study targeted to replicate varied subgrade conditions from soft to medium stiff in the test tank with a typical CBR value ranging from 2 to 5%, the CBR test molds with compacted samples were soaked (4 days) prior to the testing to replicate worst weather conditions. Based on the compaction curve, several samples were prepared by varying the moisture content at $\pm 2.0\%$ of OMC on the wet side of the curve with applied energy of 632 kN-m/m^3 . The wet side was chosen to avoid further swelling upon soaking since soil showed a minimal degree of expansiveness. Upon reaching the soaking period, the samples were examined as per the IS:2720-16 [24]. The load versus penetration plots obtained based on testing multiple repetitions (at least quadruple) are shown in Fig. 3. Besides the CBR values (2, 3 and 5%), the corresponding dry unit weights and moisture contents were recorded from the specimens, which are in the order of 16.84, 17.20 and 17.40 kN/m^3 ; 17.93, 17.60 and 17.20%, respectively.

The Base and Subbase Material

A local quarry processed aggregate material was obtained and screened to meet the gradation requirements of the Ministry of Road Transportation and Highways (MORTH)

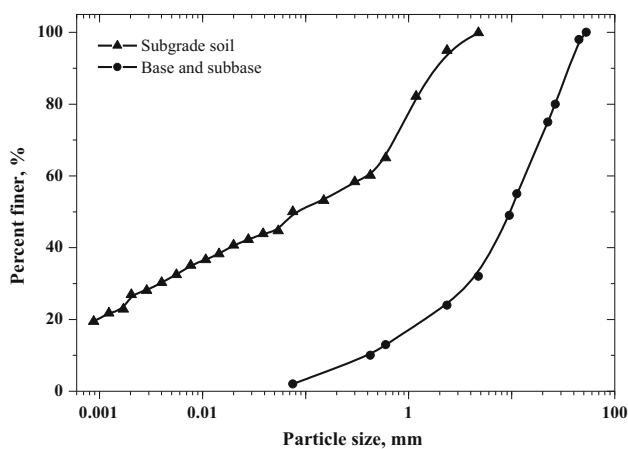


Fig. 1 The grain size distribution of subgrade and base-cum-subbase materials

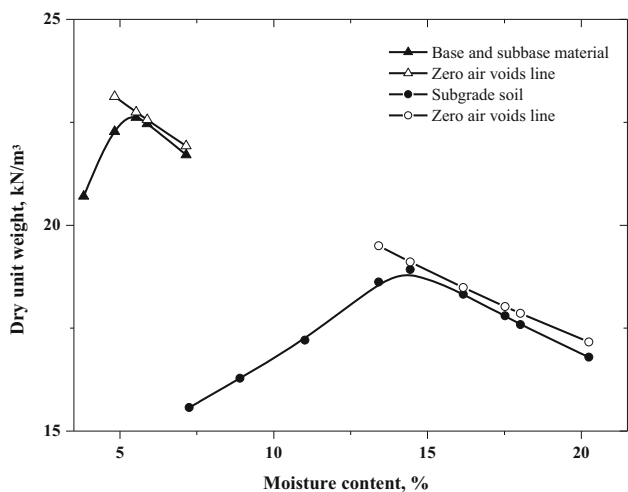


Fig. 2 Variation of dry unit weight with a moisture content of subgrade and aggregate material

[25]. The gradation of aggregate material, as shown in Fig. 1, was qualified as a base (Tab. 400-13) and subbase (Grade II) applications. The compaction characteristic curve showing the variation of the dry unit weight with moisture content is presented in Fig. 2. The modified Proctor compaction tests resulted in MDD of 22.7 kN/m³ at an OMC of 5.5%. Since the material composition is the same for both base and subbase layers, the same compaction characteristics were used.

Geogrids

Two types of geogrids made of polypropylene (GG1) and polyester (GG2) were selected for this study, as shown in Fig. 4. The geogrids, GG1 and GG2, have an ultimate tensile strengths of 30 × 30 kN/m and 60 × 60 kN/m, respectively, in the machine (MD) and cross-machine direction (CMD). These geogrids were further tested in the

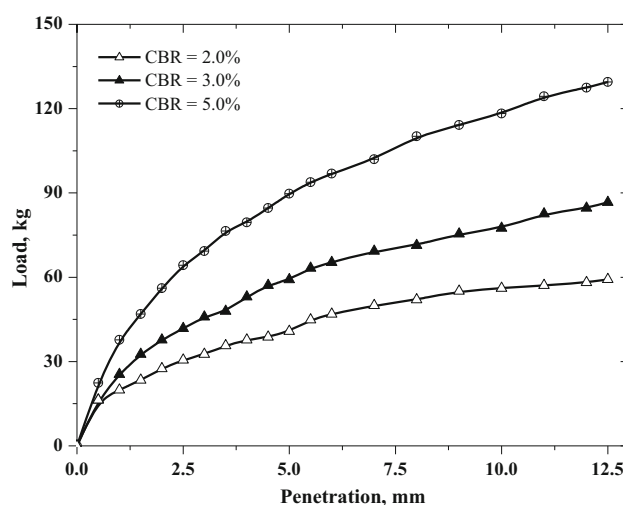


Fig. 3 The load versus penetration characteristic plot of CBR samples tested

universal testing machine for multi-rib wide width tensile tests in compliance with ASTM D6637-15 [26]. The typical tensile strength versus strain behavior of geogrids evaluated in MD and CMD are presented in Fig. 5. The GG1 and GG2 geogrids had an average stiffness of about 495 × 522 kN/m and 430 × 500 kN/m, in MD and CMD at 2% of tensile strain.

Preparation of Subgrade and Granular Layers

Before compacting the subgrade and granular layers in a test tank, calibration studies were conducted to maintain uniformly dense layers. The required subgrade material inside the test tank to maintain a particular CBR condition was divided into nearly equal parts per each lift. The weighed subgrade material for each lift (layer) construction was carefully mixed with the required moisture content, which was determined in the previous step and left to achieve equilibrium in closed airtight covers. The steps involved in the preparation of subgrade material prior to placing it inside the test tank can be found elsewhere [27]. Initially for obtaining a subgrade CBR of 2%, the required moist soil was placed in layers in the test tank measuring 1.5 m (length), 1.5 m (width) and 1.0 m (height). The required layer thickness inside the test tank for each calculated soil mass was achieved with the help of manual tamping with a wooden plank and labor maneuver for obtaining a subgrade CBR of 2%. Since the CBR of 2% possesses higher moisture content, the flowability of the moist soil is much higher when compared to the subgrade material having a CBR of 3 and 5%. Besides, to achieve the desired subgrade condition (CBR of 3 and 5%), impact compactor was traced over the test tank area with 30 min of continuous impact at 40–50 Hz frequency over each

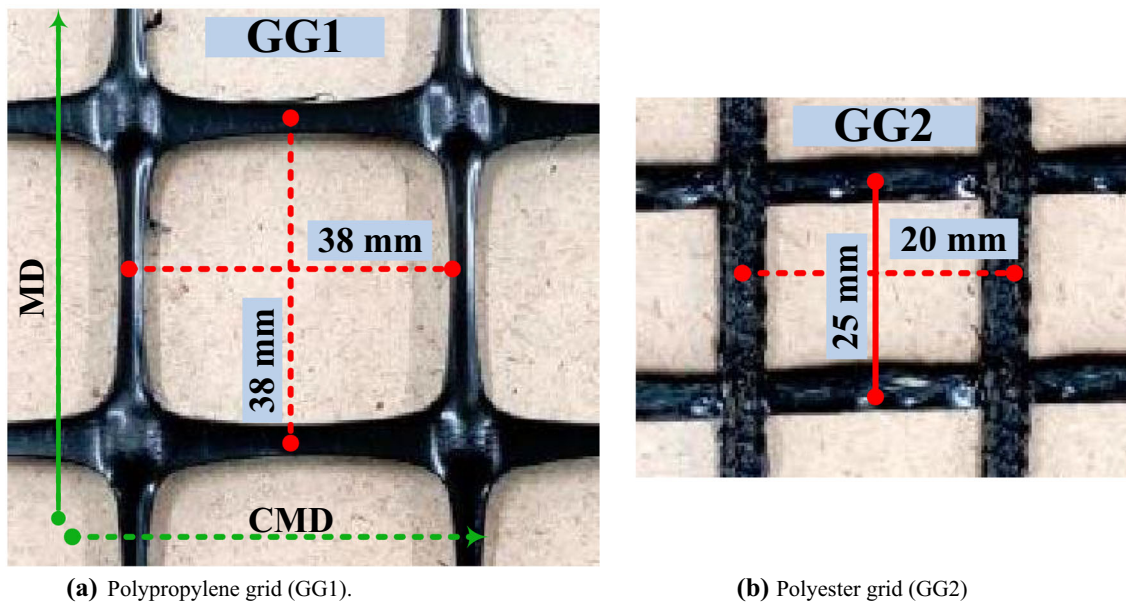


Fig. 4 Snapshot of geogrids used in the study

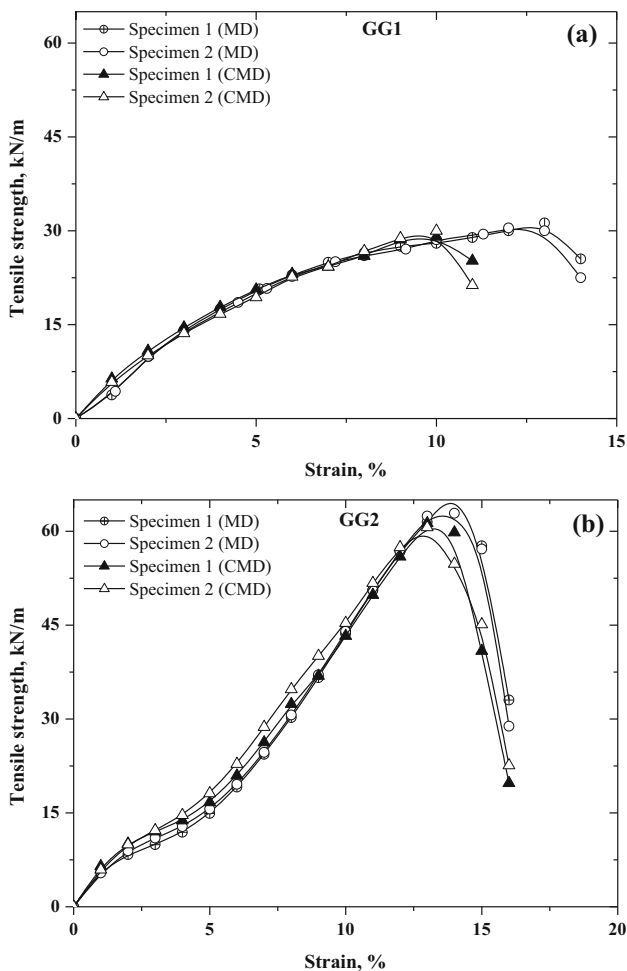


Fig. 5 The tensile characteristics of geogrids tested for a wide width multi-rib test in a universal testing machine

layer. To further enhance the compaction to the required degree, manual rammer was used. The rammer weighing 4.32 kgs with mechanized free fall from a certain height (47 cm) over a bottom impact receiving plate size of 200 mm × 200 mm was used. The CBR values of 3% and 5% were achieved at 30 min of continuous impact from the compactor and 2 and 6 passes of manual ramming over the layer, respectively. A similar procedure was followed for base and subbase layer replication to realize ideal compaction time and passes. While in the preparation of base and subbase layers inside the test tank, wet mix macadam (WMM) procedure was adopted. The resulting ideal compaction time for each layer observed with the compactor was 30 min with one round of manual ramming. The resulting compaction characteristics of each subgrade layer were ensured by extracting small core samples. However, in the case of base and subbase layers, where core samples are difficult to obtain, compaction was ensured by measuring the levels marked on the tank walls and the quantum of aggregate calculated based on the unit weight, i.e., based on weight-volume measurements.

Besides, the quality of the constructed subgrade and granular layers was assessed with the measurement of deformation modulus values using a lightweight deflectionometer (LWD). The LWD equipment with bottom impact receiving plate size of 300 mm, a falling mass of 10 kgs with the height, approximately 72 cm is used. The average measured deformation modulus values were reported to be 6.63 MN/m², 15.5 MN/m² and 16.40 MN/m² for subgrade CBR of 2%, 3% and 5%. Besides, the corresponding base and subbase measured deformation moduli values across

the height were obtained as 33 MN/m², 35 MN/m² and 39 MN/m². These measured values were further rechecked against repetitive testbeds with the same configuration to validate the obtained range of values. Any layer which was giving more than 2% error was removed and reconstructed for achieving the appropriate compaction level. It is to be noted that the preparation of testbeds, which can be replicated multiple times, is a difficult task, and of course, the key to the accurate data.

Experimental Program

It was essential to conduct static plate load tests to arrive at different benefit quantifiers such as *MIF* and *LCR*. These large-scale model pavement tests were conducted in a test tank, measuring an internal dimension of 1.5 m (length) × 1.5 m (width) × 1.0 m (height). Initially, the pavement layers which are needed to be built inside the test tank were first designed following IRC37 [28] for the traffic of two msa (million standard axles) corresponding to a given subgrade condition (CBR from 2 to 5%) as shown in Fig. 6. Experiments were conducted in three stages. The first stage of experiments was conducted to determine the elastic modulus of subgrade alone (E_2) with a complete test tank filled with subgrade material. About six tests were conducted and averaged for each case of subgrade conditions with CBR of 2%, 3% and 5%. The procedure for obtaining the resulting values of elastic modulus (E_2) of the subgrade is explained in the next section. The second stage of experiments was conducted to determine the appropriate reinforcement position in the base layer, which is to arrive at an optimum depth of geogrid placement for the highest performance. In the third stage, tests were conducted by placing the geogrid at an optimum depth to quantify the reinforcement benefits. About four numbers of tests (stage 2) were performed on the unbound pavement overlying subgrade CBR of 3% to arrive at an optimum placement depth of geogrid within the base layer. The rest of the tests (nine tests) were performed on geogrid (GG1 and GG2)-reinforced base layers over subgrade CBR of 2%, 3% and 5% (stage 3) to quantify the *MIF* and *LCR*. Firstly, a rigid circular steel plate of size 300 mm diameter and 25 mm thickness was placed concentrically on the compacted pavement layers to apply the appropriate load over the prepared test section. Over the circular plate, a ball-bearing arrangement was used to preclude the eccentric application of the load. The load was applied on the prepared testbed using a sophisticated double-acting linear dynamic actuator (100 kN capacity). The hydraulic actuator was connected to a 3.5 m high and 200 kN capacity reaction frame. The complete test setup with the prepared unbound pavement section is shown in Fig. 7. Finally, a displacement rate of

0.5 mm/min was applied on the testbed to measure the load response using a multipurpose testware graphic interface. Further data were analyzed to quantify the performance of geogrid reinforcement in terms of *MIF* and *LCR*.

Results and Discussion

Placement Depth of Reinforcement in the Base Layers

As mentioned in the earlier section, the optimum depth of geogrid for better performance was determined on a subgrade CBR of 3%. The three possible depths ($u = H_1, H_1/2$ and $H_1/3$, where “ u ” represents the geogrid depth from the top of the base layer) were examined to assess the optimum depth of geogrid in the base layer. The load response was quantified in terms of the improvement factor. Improvement factor (I_f) can be defined as the ratio of bearing pressure sustained by a geogrid-reinforced base layer overlying weak subgrade to the bearing pressure sustained by the unreinforced section, at the same elastic settlement. Figure 8 presents the improvement factors obtained over different examined placement depths of geogrid-reinforced base layers (GG1). It is evident that the reinforcement placed at one-third depth of the base layer from its top surface has resulted in the highest improvement factor of 1.44, and the least values are observed as 1.13 when the geogrid is placed at the interface of base and subbase layers. It is evident that when the geogrids are situated close to the loading region would increase the load-carrying capacity due to mobilization of membrane support from the geogrid [29, 30]. However, the attributed benefit was reduced with an increase in the placement depth. Moreover, as the depth increased, the effect of reinforcement was felt at considerably higher settlements. Therefore, further tests were carried to obtain the benefit quantifiers by placing the geogrid at the optimum depth of $H_1/3$.

Modulus Improvement Factors (MIF)

The term modulus improvement factor (*MIF*), which is defined as the ratio of the elastic modulus of the reinforced base layer to the elastic modulus of the unreinforced base layer, was used to quantify the base reinforcement effect. The following expression was used to obtain *MIF*.

$$MIF = \frac{E_{bcr}}{E_{bcu}} = \frac{E_{1r}}{E_{1u}} \quad (2)$$

where E_{bcr} is the elastic modulus of a reinforced base course (MPa) and E_{bcu} is the elastic modulus of the unreinforced base course (MPa).

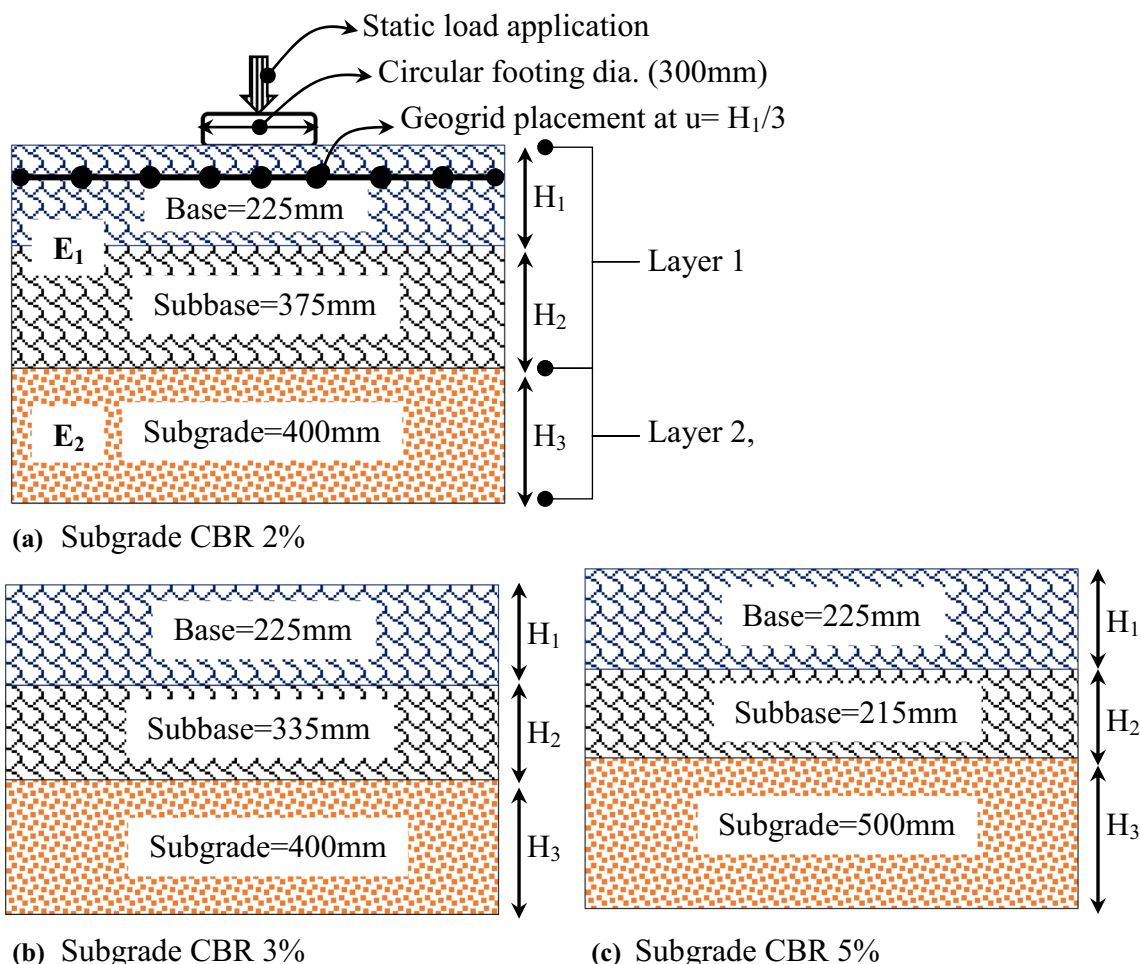


Fig. 6 Selected pavement layer thicknesses in accordance with IRC guidelines for different subgrade conditions

Since the base and subbase layers are constructed with the same materials with the same gradation, these two layers are considered as a single layer in the analysis. Now, the entire pavement, with base, subbase and subgrade layers, has become a two-layer elastic system. It is essential to obtain the individual layer elastic modulus of reinforced and unreinforced base layers to quantify the *MIF*.

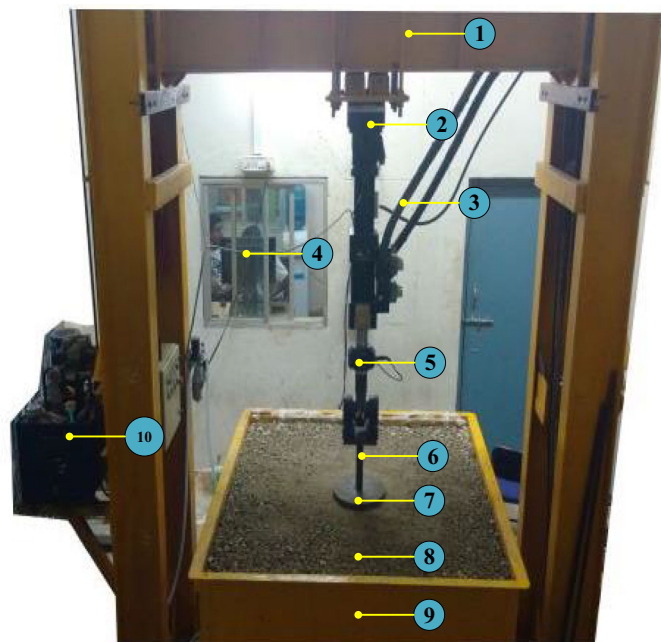
Before the determination of the elastic modulus of layer 1 (E_1), it is important to obtain an elastic modulus of subgrade (E_2). Hence, for obtaining the elastic modulus of subgrade (E_2), the following general elastic theory expression was used.

$$\text{Subgrade elastic modulus } (E_2), (\text{MPa}) = \frac{qID(1 - \mu^2)}{s_e} \tag{3}$$

where q is bearing pressure obtained from the static plate load tests at prescribed settlements, while I is the influence factor, taken as $(\mu/4)$, S_e is the elastic settlement and the D is the diameter of the plate. The Poisson's ratio (μ) of soft clay was taken as 0.4. The substitution of appropriate

values into the above equation resulted in an elastic modulus of the subgrade with a CBR of 2% as 4.7 MPa. Similarly, the subgrade with CBR of 3% and 5% resulted in about 5.4 MPa and 8.9 MPa, respectively.

Further, to obtain the elastic modulus of layer 1, the two-layer elastic approach proposed by Ueshita and Meyerhof [31] was used. Based on the modular ratio of equivalent modulus of pavement (E_{eq}) to the elastic modulus of subgrade (E_2), H/a (where H is the total height of base and subbase layers, a is the radius of the circular plate) ratio, the elastic modulus of layer one was obtained for reinforced and unreinforced sections. With the known parameters, further *MIF* values were obtained for the reinforced sections for different subgrade conditions. Table 2 presents the *MIF* values of GG1- and GG2-reinforced base layers overlying subgrades with varying values of CBR. It can be seen that the *MIF* is as high as 3.3 when the GG2-reinforced base layer was placed over a subgrade with a CBR of 2%. The lowest *MIF* was found to be 1.6 for GG1 when the subgrade condition is relatively stiff (CBR = 5%). The improved modulus was observed to be



Experimental key components

1. Test frame (20 Ton capacity)
2. Actuator
3. Hose pipes
4. Test control and monitor
5. Load cell (100 kN)
6. Plunger
7. Rigid circular plate (Dia.300mm)
8. Prepared test section
9. Test chamber (1.5m×1.5m×1.0m)
10. Actuator shifting control unit

Fig. 7 Large-scale model pavement test setup

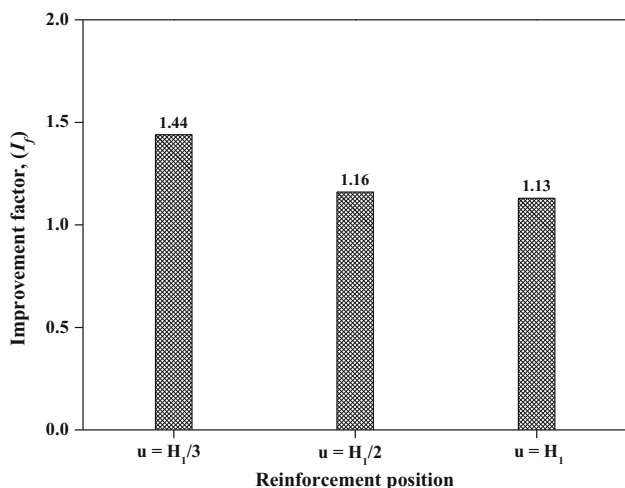


Fig. 8 Variation of improvement factor (*I_f*) with placement depth of reinforcement (*u*) within the base layer

higher for a combination of low subgrade condition (CBR 2%) and higher tensile strength of geogrid, and, as the subgrade condition changes to a relatively stiffer nature (CBR 5%), the *MIF* values reduced. In other words, for a given subgrade condition, the *MIF* was found higher if the tensile strength of the geogrid was higher. The improvement in *MIF* might be due to the reinforcement effect of the geogrid as the resistance to the deformation offered by the subgrade is lower. On the other hand, the lower *MIF* values might have resulted due to the stiff nature of the subgrade, which might not have offered better resistance to deformation.

Layer Coefficient Ratios (LCR)

Generally, *LCRs* are back-calculated based on experimentally evaluated *MIF* values. The *LCR* equation (Eq. 4) suggested by Giroud and Han [15], which is modified based on the AASHTO [11] base layer coefficient equation (Eq. 1), is used to obtain the *LCR* through *MIF*. The AASHTO [11] equation gives the base layer coefficient corresponding to a base layer resilient modulus. The regression model was proposed based on the field data observed from the AASHTO road tests conducted in the late 1950s. Hence, the applicability of the model for a wide range of subgrade conditions is questionable and warrants for a design verification before it is adopted for the reinforced base layers, generally selected for weak subgrade conditions (CBR between 2% and 5%).

$$LCR = \frac{0.249 \times \log_{10}(MIF \times \frac{M_{ru}}{0.0069}) - 0.977}{0.249 \times \log_{10}(\frac{M_{ru}}{0.0069}) - 0.977} \tag{4}$$

where *M_{ru}* is the resilient modulus of the unreinforced base layer in MPa.

The following section emphasizes on the formulation and determination of unreinforced and reinforced base layer coefficients.

Determination of New Base Layer Coefficients

A three-layer elastic system was considered for the determination of the base layer coefficient of unreinforced and geogrid-reinforced pavement sections. As discussed in the

Table 2 The modulus improvement factors (*MIF*) of geogrid (GG1 and GG2)-reinforced bases

Geogrid	Subgrade condition	<i>MIF</i>
GG1	CBR 2%	2.40
GG1	CBR 3%	1.88
GG1	CBR 5%	1.60
GG2	CBR 2%	3.33
GG2	CBR 3%	2.25
GG2	CBR 5%	2.00

earlier section, a combined pavement analysis approach, the structural number-based AASHTO [11] design, along with damage analysis, was carried out. The structural number represents the total pavement thickness, and damage analysis ensures the selected pavement safety against fatigue (horizontal tensile strains below the asphalt layer) and rutting (vertical compressive strain on top of subgrade layer) strains. The following Eq. 5 gives the expression for computing the structural number.

$$S_N = (a_1 \times d_1)_{\text{asphalt layer}} + (a_2 \times d_2 \times m_2)_{\text{base}} \quad (5)$$

where S_N is the required structural number, a_1 and a_2 are layer coefficients of asphalt and base layers, d_1 and d_2 are asphalt and base layer thicknesses and m_2 is the drainage coefficient of the base layer.

In the present study, the analysis was conducted for the traffic as 2, 5, 10, 20, 30, 40, 50, 100 and 150 msa and subgrade with a CBR of 2%, 3%, 4% and 5%. Initially, required structural number, S_N was calculated using the AASHTO nomograph (W_{18} , anticipated cumulative 18-kip equivalent standard axles (ESAL)) for a selected subgrade resilient modulus. The parameters, reliability of 90%, standard normal deviate (Z_R) of -1.282 , overall standard deviation (S_o) of 0.49, allowable loss (Δ PSI) of serviceability as 2.2 and underlying subgrade resilient modulus (M_{rs}) of 3046, 4496, 6091 and 7542 psi corresponding to CBR of 2%, 3%, 4% and 5%, respectively, were used to compute the required structural number based on a trial and error method. All the calculated structural numbers for various traffic and subgrade conditions were stored.

For an asphalt layer, a_1 and d_1 values were obtained from AASHTO [11] guidelines as $a_1 = 0.43$ for an asphalt layer resilient modulus of 3000 MPa. The asphalt layer thickness d_1 was ranged from 75 to 110 mm, and these thicknesses were within the range specified by AASHTO guidelines. The minimum asphalt thickness (75 mm) was assigned for lower traffic (2 msa), and higher thickness (110 mm) was assigned for higher traffic (150 msa). The drainage coefficient (m_2) of the base layer was taken as 1.0. Similarly, a practical range of resilient modulus of a virgin aggregate (200 MPa to 350 MPa) collected across the

world by Peddinti et al. [32] was adopted for the current study. To compute the base layer thickness with all other known parameters, a pavement analysis program, KENPAVE was used.

To arrive at an appropriate base layer thickness (d_2) based on the traffic, subgrade type and material data input, thickness satisfying the horizontal tensile strains (fatigue, ϵ_t) below the asphalt layer and vertical compression strain (rutting, ϵ_v) on the top of subgrade was considered. The critical strain equations adopted by IRC:37 [18] based on the Asphalt Institute manual were used for 90% reliability to compute limiting fatigue strains. Besides, Poisson's ratio of asphalt, base and subgrade was inputted as 0.35, 0.35 and 0.4, respectively. All the layers were considered as interface bonded. Total 144 pavement sections were analyzed with a trial base layer thickness in each case that satisfies the limiting strains were stored. Now, with all known data, the base layer coefficient of an unreinforced base layer can be computed by rearranging Eq. 5, as shown in Eq. 6.

$$a_{2u} = \frac{S_N - (a_1 \times d_1)_{\text{asphalt layer}}}{(d_2 \times m_2)_{\text{base}}} \quad (6)$$

A flow chart showing steps followed for obtaining the base layer coefficients is shown in Fig. 9. Further, regression analysis was performed to get the base layer coefficient of the unreinforced section as a function of resilient modulus. Figure 10 shows the variation of the unreinforced base layer coefficient with the resilient modulus of the base course material. A newly proposed model for obtaining the base layer coefficient of an unreinforced section for varied subgrade conditions (CBR = 2 to 5%) is shown in Eq. 7.

$$a_{2u} = 0.224 \times \log_{10}(M_{ru}) - 0.365 \quad (7)$$

where a_{2u} is the unreinforced base layer coefficient, M_{ru} is the resilient modulus of the unreinforced base layer in MPa.

The above equation has shown an excellent correlation with a coefficient of determination (R^2) of 0.99. Further, for reinforced sections, a similar procedure was followed by keeping all the parameters constant except the input value of the resilient modulus, which attributes due to the reinforcement effect. Total 576 reinforced pavement sections were analyzed. To quantify the reinforcement effect, *LCR* was taken into consideration where the benefit was observed in terms of improved resilient modulus. Initially, the reinforced base layer coefficient was computed by multiplying the *LCR* to the unreinforced base layer coefficient, as shown in Eq. 8. In the present study, *LCR* was varied from 1.2 to 1.7.

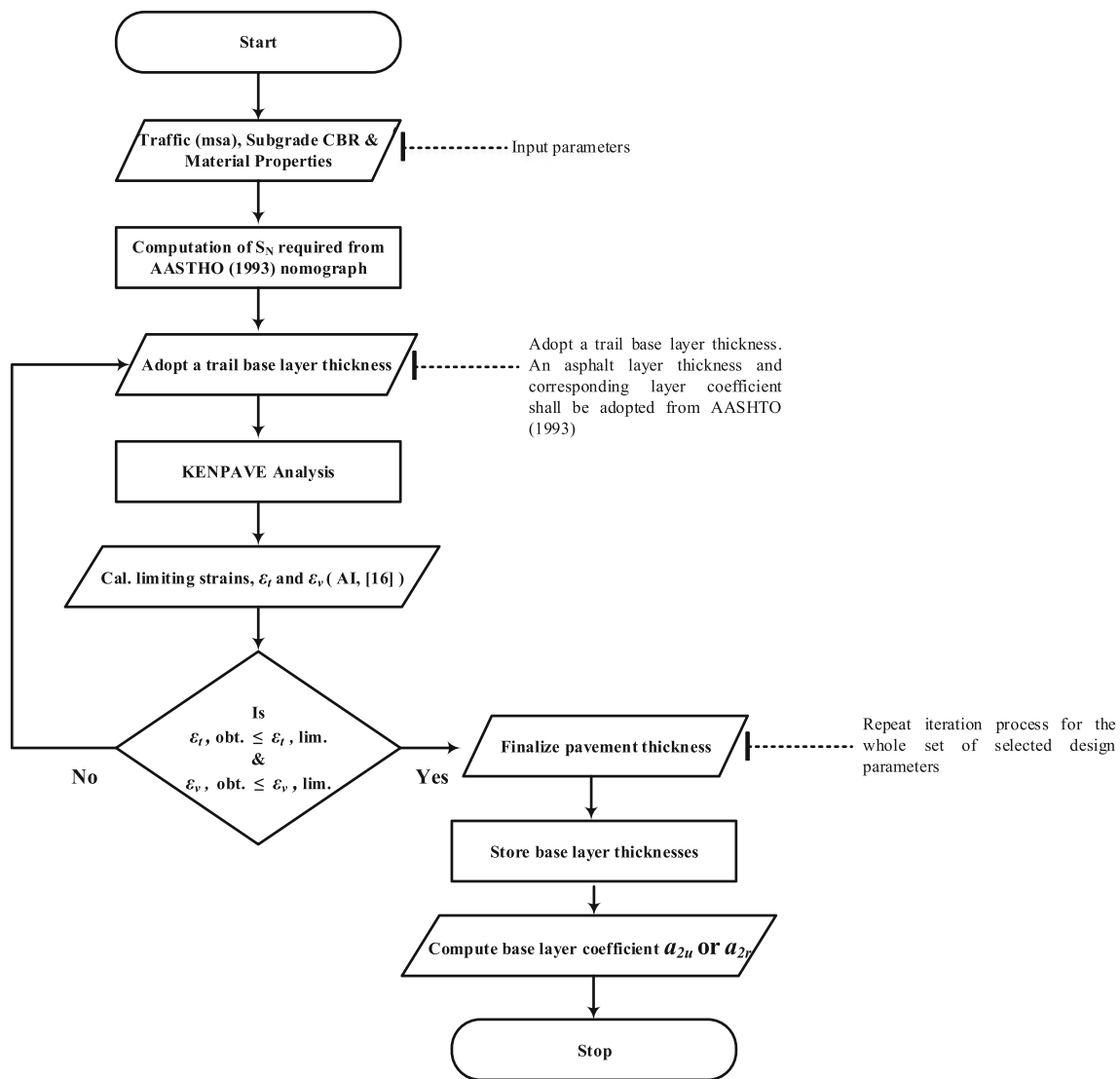


Fig. 9 Flow chart showing the sequence of steps followed while computing the base layer coefficients

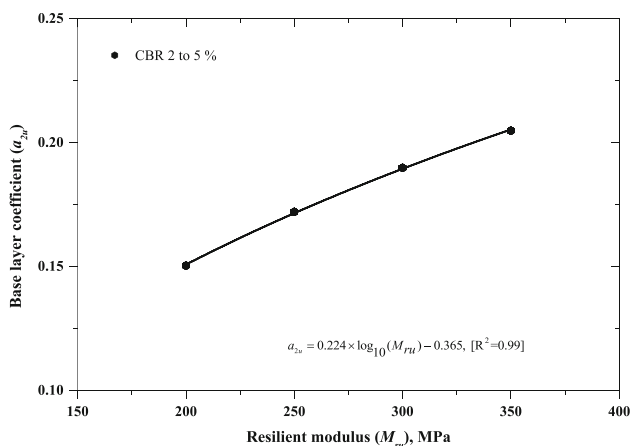


Fig. 10 Variation of unreinforced base layer coefficient with base layer resilient modulus

The improved $a_{2r} = LCR \times a_{2u}$ (IRC : SP59 : [12]) (8)

The obtained a_{2r} is substituted into Eq. 7 to obtain the improved resilient modulus, and this typical procedure explained in detail in IRC: SP59: [12]. For all selected range of LCR values, the improved modulus values were inputted into the KENPAVE for obtaining reduced thicknesses of the base layer, which satisfy the critical strains. Further, the reinforced base layer coefficient is computed by using Eq. 9:

$$a_{2r} = \frac{S_N - (a_1 \times d_1)_{\text{asphalt layer}}}{(d_{2r} \times m_2)_{\text{base}}} \tag{9}$$

where a_{2r} is the reinforced base layer coefficient, and d_{2r} is the reduced base layer thickness.

Regression analysis was carried out to obtain the reinforced base layer coefficient as a function of known

unreinforced resilient modulus and LCR values. The proposed equation to obtain the base layer coefficient of the geogrid-reinforced section for a given subgrade with CBR between 2 and 5% is shown in Eq. 10.

$$a_{2r} = 0.0142 \times [\log_{10}(M_{ru})]^{2.876} \times (LCR)^{0.960} \quad (10)$$

The newly developed single equation (Eq. 10) for a selected range of subgrade conditions showed an extremely high correlation for the chosen range of values with a high coefficient of determination ($R^2 = 1.0$). The equation directly provides the reinforced base layer coefficient if the resilient modulus of unreinforced layer and the LCR values are known, to calculate the base layer thickness. However, to obtain the a_{2r} , either Eq. 8 or 10 may be used. To simply further, a chart is proposed to directly obtain the geogrid-reinforced base layer coefficient (a_{2r}) for a given LCR and M_{ru} (Fig. 12). It is crucial to validate the newly developed equations for unreinforced and reinforced base layer coefficients before adopting them in the design of flexible pavements with geogrid-reinforced bases.

Model Validation

To validate the proposed model for reinforced base layer coefficients, the layer coefficient ratios are obtained from Eq. 11, and are compared with the LCR values computed from Giroud and Han [15] method (Eq. 4). In the analysis, the MIF values obtained from the large-scale experiments conducted on GG1- and GG2-reinforced base layers overlying different subgrade conditions (Table 2) are used. The resilient modulus of aggregate, M_{ru} of 323 MPa, obtained from a resilient modulus test conducted in the laboratory, was considered in the analysis.

$$LCR = \frac{0.244 \times \log_{10}(MIF \times M_{ru}) - 0.365}{0.244 \times \log_{10}(M_{ru}) - 0.365} \quad (11)$$

Figure 11 compares the variation of LCR with a change in the subgrade condition from the present study and Giroud and Han [15]. Higher LCR values were observed for weaker subgrade conditions (CBR 2%), and as the subgrade condition improves relatively to stiffer, the LCR values decreased. However, the substantial benefit was witnessed for a geogrid with higher tensile strength (GG2) than the geogrid (GG1) with lower tensile strength. Nevertheless, the LCR values computed from the Giroud and Han [15] and the newly proposed equation ranged between 1.27–1.7 and 1.23–1.59, respectively. The LCR values calculated from the proposed equation are slightly on the lower side than Giroud and Han [15] equation. It is important to note that a small change in the LCR value may make a difference in obtaining the pavement layer thickness. For example, a higher LCR generally indicates a reduced thickness due to which the actual thickness range

could be missed with the overestimated LCR value. Also, the reduced thicknesses, if not tested for critical strains, may lead to severe pavement damage in terms of rutting or fatigue.

To further validate the models proposed for both unreinforced and geogrid-reinforced base layers, an example is considered to analyze a pavement section. The design was performed based on the AASHTO [14] method considering the LCR evaluated from both the approaches. A subgrade condition of CBR 2% with design traffic of 50 msa was considered for the design. Table 3 shows the design example validation for unreinforced and geogrid-reinforced pavements. The selected design parameters, such as traffic, subgrade condition, required structural number, etc. are listed in Table 3. From Table 3, it can be seen that both the design methods obtained layer thicknesses do not show failure in terms of critical strains. However, considerable differences were observed in the case of the unreinforced section. The AASHTO equation yielded a base layer thickness of about 818 mm. Whereas for the newly proposed equation yielded a base layer of thickness 767 mm. It is noteworthy to consider that the AASHTO method suggests a conservative thickness for the base layer. The present model ensured the safety of the pavement against fatigue and rutting failure modes as well as the structural number approach.

In the case of the geogrid-reinforced section, a MIF value of 2.5 was considered so as to obtain the LCR values of 1.47 and 1.56 from the present study and from Giroud and Han [15], respectively. These values are presented in Table 3. It is evident that LCR equal to 1.56 resulted in a reduced thickness of the unreinforced base layer from 818 to 524 mm. Whereas from the present study ($LCR = 1.47$), the thickness was reduced from 767 to 521 mm. Both the methods satisfied the critical fatigue and rutting strains with the proposed design thicknesses. Due to the marginal

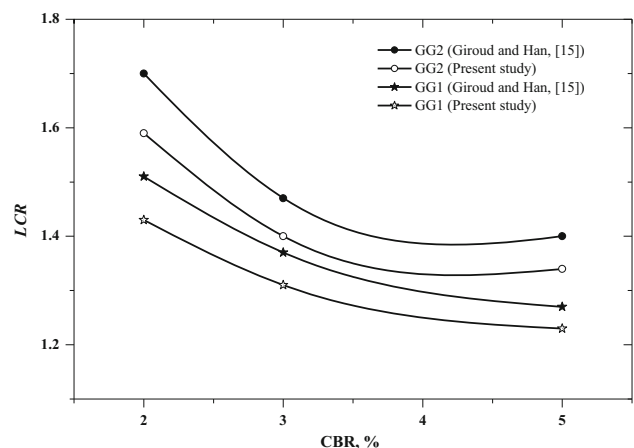


Fig. 11 LCR variation with subgrade CBR of present study and Giroud and Han [15]

Table 3 Design example and validation for geogrid-reinforced pavement sections with the proposed new a_{2u} and a_{2r} equation

S.no.	Pavement particulars	AASHTO [11]	Present study
1	Subgrade CBR	CBR 2%	CBR 2%
2	Million standard axles	50 msa	50 msa
3	Asphalt layer		
	Resilient modulus, M_{ra} (MPa)	3000	3000
	Thickness, d_1 (mm)	110	110
	Layer coefficient (a_1)	0.43	0.43
4	Unreinforced base layer		
	Resilient modulus, M_{ru} (MPa)	300	300
	Drainage coefficient (m_2)	1.0	1.0
	Layer coefficient (a_{2u})	0.1780 (Eq. 1)	0.1898 (Eq. 7)
	Thickness ^a , d_2 (mm)	818	767
5	S_N (required)	7.594	7.594
	S_{Na} (actual)	7.594	7.594
	S_{Na} (actual) $\geq S_N$ (required)	Safe	Safe
6	Fatigue strain, ϵ_t (Limiting = 0.00017813)	– 0.00020998	– 0.0002100
	Rutting strain, ϵ_v (Limiting = 0.00037169)	0.00021580	0.0002394
7	Reinforced base layer		
	Resilient modulus, M_{ru} (MPa)	300	300
	Improved resilient modulus, M_{rr} (MPa)	750	750
	Drainage coefficient (m_2)	1.0	1.0
	Modulus improvement factor (<i>MIF</i>)	2.5	2.5
	Layer coefficient ratio (<i>LCR</i>)	1.56 (Eq. 4)	1.47 (Eq. 11)
	Layer coefficient (a_{2r})	0.2777	0.2792 (Eq. 10)
	Thickness ^a , d_{2r} (mm)	524	521
8	S_N (required)	7.594	7.594
	S_{Na} (actual)	7.594	7.594
	S_{Na} (actual) $\geq S_N$ (required)	Safe	Safe
9	Fatigue strain, ϵ_t (Limiting = 0.00017813)	– 0.00010520	– 0.0001057
	Rutting strain, ϵ_v (Limiting = 0.00037169)	0.00024550	0.00024770
	Reinforced base layer (<i>LCR</i> = 1.2)		
10	Resilient modulus, M_{ru} (MPa)	300	300
	Improved resilient modulus, M_{rr} (MPa)	417	443
	Drainage coefficient (m_2)	1.0	1.0
	Layer coefficient ratio (<i>LCR</i>)	1.2	1.2
	Layer coefficient (a_{2r})	0.2136	0.2297
	Thickness ^a , d_{2r} (mm)	682	634
11	S_N (required)	7.594	7.594
	S_{Na} (actual)	7.597	7.595
	S_{Na} (actual) $\geq S_N$ (required)	Safe	Safe
12	Fatigue strain, ϵ_t (Limiting = 0.00017813)	– 0.00016930	– 0.00016050
	Rutting strain, ϵ_v (Limiting = 0.00037169)	0.00023530	0.00025150

^aThe thickness shown is a combined thickness of base and subbase layers. The individual thickness of base layer may be considered about 40% of the thickness shown

difference in the *LCR* values from both the methods, the resulting thicknesses are found to be nearly the same. However, in the absence of the *LCR* values from the

manufacturer or large-scale testing, as per the IRC SP59 [16], the designer is supposed to adopt an *LCR* of 1.2 for geogrids. In such a case, the Giroud and Han [15] method

gives a conservative base layer thickness which is about 8–10% higher than the value given by the proposed model (Table 3).

The present model resulted in about a 33% reduction in the base layer thickness when compared to the unreinforced section. The significant advantage of the present study is that the designer can directly obtain the geogrid-reinforced base layer coefficient from the proposed model without further evaluation of critical strains since base layer thicknesses were already assessed for the critical strains.

Design Charts

A chart is presented based on the new model, as shown in Fig. 12, to obtain the base layer coefficient of geogrid-reinforced base layer as a function of LCR (varied from 1.2 and 1.5) and unbound base layer resilient modulus, M_{ru} . Since the chart is proposed based on the practical range of LCR , resilient modulus of unreinforced bases, and for a set of subgrade conditions, the base layer coefficients can be directly obtained to calculate the reinforced base layer thicknesses. The reinforced base layer coefficients are found to increase logarithmically with an increase in traffic and resilient modulus of the base layer. Besides, for a given resilient modulus, higher a_{2r} values are found for higher LCR values, irrespective of the subgrade condition. The a_{2r} values ranged from 0.18 to 0.31 for M_{ru} between 200 MPa and 350 MPa, respectively. Further, a typical design chart (Fig. 13) to obtain the granular (base and subbase) layer thickness as a function of design traffic, unreinforced resilient modulus and LCR for a subgrade CBR of 2% is presented. Similar charts can be proposed for other subgrade conditions. The layer thickness shown in this chart is a combined thickness of base and subbase layers. From the large-scale experiments, it can be suggested that the base layer may be considered as 40% of the total thickness obtained from Fig. 13.

It is to be noted that the a_{2r} values are not provided for $LCR = 1.7$. It is due to the demand for very high base layer resilient modulus (> 500 MPa), which would lead to an impractically high improved resilient modulus of the base layer at $LCR = 1.7$. To understand this behavior, improved resilient modulus values are back-calculated from different LCR values and summarized in Table 4. It can be seen that for an unreinforced resilient modulus of 400 MPa with $LCR = 1.7$, the improved values of resilient modulus of the base layer are found to be more than 1900 MPa. A simple back-analysis shows that the resulting MIF value for such a high improved resilient modulus is about 4.8, which is not practical to obtain with the geogrids tested (Table 2). Besides, such a high value of resilient modulus is not practically achievable for a reinforced base layer, assuming

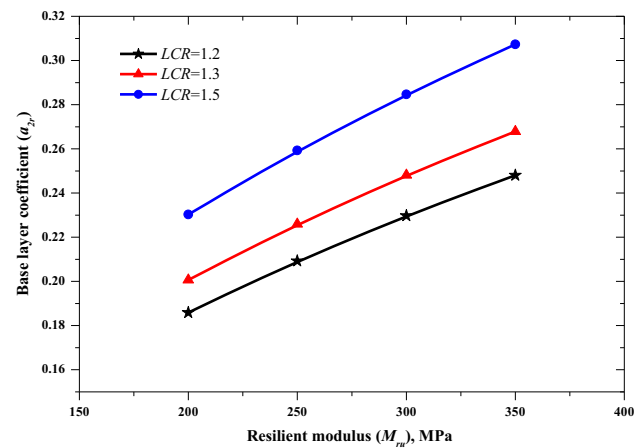


Fig. 12 Variation of reinforced base layer coefficient with resilient modulus of base material

this could tend to a fatigue failure of the pavement owing to the stiff nature of the layer. At the same time, it is ideal to consider an appropriate unreinforced resilient modulus value for higher design traffic. However, it is not always possible to obtain an unreinforced resilient modulus of more than 400 MPa in the field without adopting any stabilizing methods. From these observations, it is also convincing that the proposed models to calculate the base layer coefficients are more practical. Hence, to overcome this issue, it is always advisable to adopt a direct approach to design flexible pavements with geogrid-reinforced base layers.

Conclusions

An attempt has been made in the present study to propose a new set of equations for calculating the base layer coefficients for both unreinforced and geogrid-reinforced base layers through a regression analysis conducted on a three-layer elastic system. Besides, a series of large-scale model pavement experiments (LSMPE) were conducted to determine the range of MIF and LCR values for different geogrids and subgrade conditions, and these experimental ranges were considered appropriate in the design aspects. The following important conclusions can be drawn from the present study.

- The MIF value for the geogrid-reinforced base layers was found to range between 1.6 and 3.33 for GG1 and GG2 geogrids over the subgrade CBR of 2–5%.
- Higher MIF values are noticed when the higher tensile strength of geogrid is adopted in base layer over a weak subgrade condition (CBR = 2%).
- The computed LCR values of existing (proposed by Giroud and Han, [15]) and newly proposed equations

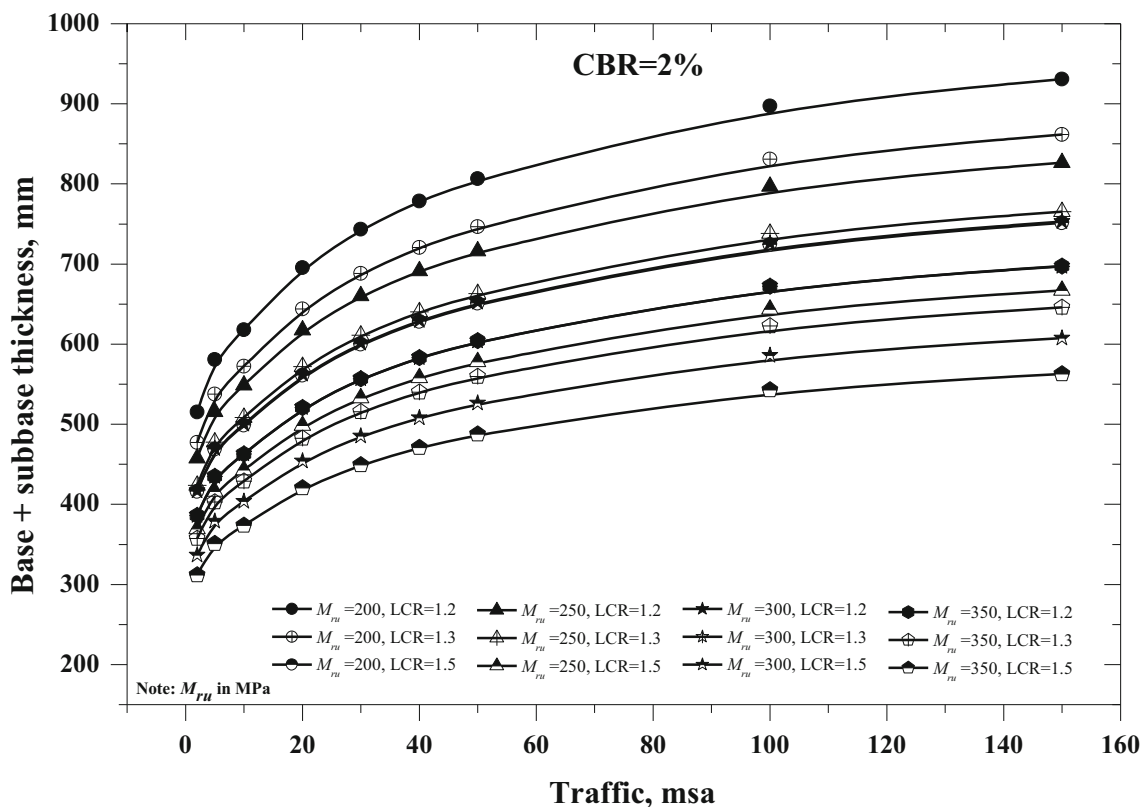


Fig. 13 Typical design chart showing base and subbase thicknesses for a range of traffic, resilient modulus and LCR values

Table 4 Improved resilient modulus (M_{rr}) for the select combination of LCR and unreinforced resilient modulus of the base course

Resilient modulus (M_{ru})	LCR	Improved resilient modulus (M_{rr})
300	1.2	443
	1.3	539
	1.5	796
	1.7	1176
400	1.2	626
	1.3	783
	1.5	1226
	1.7	1918

ranged between 1.27–1.7 and 1.23–1.59, respectively. The existing method slightly overestimated the LCR values by adopting the AASHTO-based base layer coefficients.

- Further, to compute the base layer coefficient of unreinforced and geogrid-reinforced base sections, the following simplified new expressions are proposed for soft subgrade conditions with CBR varied between 2 and 5%.

$$a_{2u} = 0.224 \times \log_{10}(M_{ru}) - 0.365$$

$$a_{2r} = 0.0142 \times [\log_{10}(M_{ru})]^{2.876} \times (LCR)^{0.960}$$

- A design section was validated by computing the structural numbers as well as the critical strains (fatigue and rutting). The existing design methods [11, 12] suggest a conservative unreinforced base layer thickness.
- A typical design chart is provided to obtain the base layer thickness for a given design traffic, LCR and base layer resilient modulus.
- It is recommended to use LCR values up to 1.5 for the design purposes in the case of stiffer subgrade condition (CBR 5%) and an unreinforced resilient modulus up to 400 MPa.

Acknowledgements This research work has been carried out under active funding from the national highway authority of India (NHAI). The authors are thankful for NHAI. Authors also extend their gratitude for TechFab India Ltd. and Strata (I) Geosystems Ltd. for providing material for the study. The authors would like to thank Prof. M. R Madhav and Dr. B. Umashankar for providing valuable inputs during the experimental program.

Compliance with Ethical Standards

Conflict of interest The authors declare that they have no conflict of interest.

References

- Berg RR, Christopher BR, Perkins S (2000) GMA white paper II, Geosynthetic reinforcement of the aggregate base/subbase courses of pavement structures, AASHTO committee 4E, prepared by geosynthetic material association
- Giroud JP, Han J (2004) Design method for geogrid-reinforced unpaved roads II. calibration and applications. *J Geotech Geoenviron Eng* 130(8):787–797. [https://doi.org/10.1061/\(ASCE\)1090-0241\(2004\)130:8\(787\)](https://doi.org/10.1061/(ASCE)1090-0241(2004)130:8(787))
- Montanelli F, Zhao A, Rimoldi P (1997) Geosynthetic-reinforced pavement system: testing and design. In: *Geosynthetics'97 conference*, pp 1–15
- Hufenus R, Rueegger R, Banjac R, Mayor P, Springman SM, Brönnimann R (2006) Full-scale field tests on geosynthetic reinforced unpaved roads on soft subgrade. *Geotext Geomembr* 24(1):21–37. <https://doi.org/10.1016/j.geotexmem.2005.06.002>
- Christopher BR (2016) Geotextiles used in reinforcing paved and unpaved roads and railroads. *Geotextiles*. <https://doi.org/10.1016/B978-0-08-100221-6.00014-0>
- Han J (2013) Design of planar geosynthetic-improved unpaved and paved roads. *Pavement Geotech Eng Transp*. <https://doi.org/10.1061/9780784412817.003>
- Korulla M, Gharpure A, Rimoldi P (2015) Design of geogrids for road base stabilization. *Indian Geotech J* 45(4):458–471. <https://doi.org/10.1007/s40098-015-0165-3b>
- Perkins PS, Christopher BR (2012) Evaluation of AASHTO'93 layer coefficients for pavements reinforced with NAUE geogrids. Final project report, pp 1–16
- Goud GN, Ramu B, Umashankar B, Sireesh S, Madhav MR (2020) Evaluation of layer coefficient ratios for geogrid-reinforced bases of flexible pavements. *J Road Mater Pavement Des*. <https://doi.org/10.1080/14680629.2020.1812424>
- Zhao A, Foxworthy TP (1999) Geogrid reinforcement of flexible pavements: a practical perspective. *Technical Reference GRID-DE-6*. p. 1–15
- AASHTO (1993) *Guide for design of pavement structures*. American association of state highway and transportation officials, Washington, DC
- IRC: SP-59 (2019) *Guidelines for use of geosynthetics in road pavements and associated works*. First revision, Indian Road Congress
- Rimoldi P (2019) Design methods for base stabilization of paved roads. *Geotech Transp Infrastruct Lect Notes Civ Eng* 28:51–80. https://doi.org/10.1007/978-981-13-6701-4_3
- AASHTO R50–09, (2013) *Standard practice for geosynthetic reinforcement of the aggregate base course of flexible pavement structures*, 35th edn. AASHTO, Washington, D.C.
- Giroud JP, Han J (2013) Design of geosynthetic-reinforced unpaved and paved roads. Short course, *Geosynthetics 2013*, Long Beach, CA, April 4
- Asphalt Institute, MS-2 (2014) *Asphalt mix design methods*, 7th edn. Lexington, Asphalt Institute
- Huang YH (2004) *Pavement analysis and design*. Pearson Prentice Hall, Cambridge, pp 490–491
- IRC 37 (2018) *guidelines for the design of flexible pavements*, 4th edn. Indian Road Congress, Delhi
- IS 2720-3-2 (1980) *Methods of test for soils, part 3: determination of specific gravity, section 2: fine, medium and coarse-grained soils*, Reaffirmed 2002, CED 43: soil and foundation engineering
- IS 2720-5 (1985) *Methods of test for soils, Part 5: Determination of liquid and plastic limit*. Reaffirmed 2006, CED 43: Soil and Foundation Engineering
- IS 2720-40 (1977) *Methods of test for soils, Part 40: Determination of free swell index of soils*. Reaffirmed, 2002, CED 43: Soil and Foundation Engineering
- IS 2720-7 (1980) *Methods of test for soils, Part 7: Determination of water content-dry density relation using light compaction*. Reaffirmed 2011, CED 43: soil and foundation engineering
- IS 1498 (1970) *Classification and identification of soils for general engineering purposes*. Reaffirmed, 2007, CED 43: soil and foundation engineering
- IS 2720-16 (1987) *Laboratory determination of CBR, methods of test for soils*. Reaffirmed, 2002, CED 43: soil and foundation engineering
- MORTH (2013) *Specifications for road and bridge works*, 5th edn. Ministry of Road Transport and Highways, Delhi
- ASTM D6637/D6637M (2015) *Standard test method for determining tensile properties of geogrids by the single or multi-rib tensile method*. <https://compass.astm.org>
- Saride S, Sitharam TG, Dash SK (2009) Bearing capacity of circular footing on geocell-sand mattress overlying clay bed with void. *Geotext Geomembr* 27:89–98
- IRC 37 (2012) *Guidelines for the design of flexible pavements (3rd Revision)*. Indian Road Congress, Delhi
- Binquet FJ, Lee KL (1975a, b) Bearing capacity of reinforced earth slabs. *ASCE J Geotech Eng* 101(GT12): 1241–1255, 1257–1275
- Sitharam TG, Saride S (2004) Model studies of embedded circular footing on geogrid reinforced sand beds. *Ground Improvement* 8(2):69–75
- Ueshita K, Meyerhof GG (1967) Deflection of multilayer soil system. *J Soil Mech Found Div ASCE* 93(SM5):257–282
- Peddinti PRT, Basha BM, Saride S (2017) Probability density functions associated with the resilient modulus of virgin aggregate bases. *Geotech Spec Publ*. <https://doi.org/10.1061/9780784480441.033>

Publisher's Note Springer Nature remains neutral with regard to jurisdictional claims in published maps and institutional affiliations.